Catalysis Letters (2021) 151:2027–2037
https://doi.org/10.1007/s10562-020-03432-4

The Ultra-Deep Desulfurization of Model Oil Using Amphipathic Lindqvist-Type Polyoxometalate-Based TiO_2 Nanofibres as Catalysts

Jiawei Fu[1] · Wenwen Ma[1,2] · Yu Guo[1] · Xiaonan Li[1] · Haiyu Wang[1] · Chen Fu[1] · Hong Zhang[1]

Received: 24 July 2020 / Accepted: 16 October 2020 / Published online: 3 November 2020

Abstract

A new amphipathic lindqvist-type polyoxometalate-based TiO_2 nanofibres catalysts (**50-DTA-MoO-TiO_2 NF**, DTA = $CH_3(CH_2)_{11}(CH_3)_3N$, MoO = $Mo_6O_{19}^{2-}$, TiO_2 NF = TiO_2 nanofibres, the weight percentage of DTA-MoO was 50%) was obtained by electrospinning and applied in desulfurization of fuel. This catalyst presented outstanding desulfurization performance and reusability.

Graphic Abstract

The amphipathic lindqvist-type polyoxometalate-based TiO_2 nanofibres were prepared successfully and examined as heterogeneous catalysts in removal of sulfur-containing compounds. At 333 K, 100% desulfurization efficiency of 500 ppm DBT model oil was achieved using 0.010 g **50-DTA-MoO-TiO_2 NF** as catalyst in 40 min with O/S molar ratio of 2:1 in ECODS.

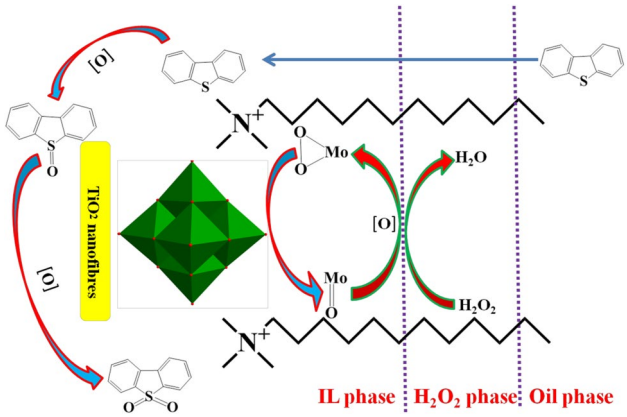

Keywords Amphipathic catalysts · Nanofibres · Electrospinning · Clean fuels

1 Introduction

With increasingly stringent standards of fuels quality, tremendous attention has been paid to researching in efficient desulfurization techniques to obtain fuels with ultra-low sulfur content [1]. Hydrodesulfurization (HDS) can remove the aliphatic and acyclic sulfur compounds, however, the application of HDS is restricted because of harsh reaction conditions and less effective for heterocyclic sulfur compounds [2]. At present, extractive catalytic oxidative desulfurization (ECODS) has become a hot research subject due

Electronic supplementary material The online version of this article (doi:https://doi.org/10.1007/s10562-020-03432-4) contains supplementary material, which is available to authorized users.

✉ Wenwen Ma
mwwbhu@sina.com

✉ Hong Zhang
hope20130122@163.com; zhangh@nenu.edu.cn

Extended author information available on the last page of the article

to its cost-effectiveness and no hydrogen consumption [3, 4]. In ECODS, oxidant and catalysts play an importance roles. H_2O_2 is the most extensively adopted oxidant due to high availability and environmental compatibility [5]. Developing high active catalysts to obtain clean-oil is very vital for the industrial application of ECODS [6].

Polyoxometalates (POMs) catalysts are widely used in removing organic substrates in view of its extraordinary physicochemical properties, high activity and environmentally friendly [7, 8]. Whereas, the low recyclability greatly hinders the practical industrial application of these catalysts. In order to overcome this issue, many methods have been proposed to fabricate POMs-based heterogeneous catalysts. Heterogeneous catalysts with excellent recyclability is considered as promising candidates for green catalytic application [9, 10]. For instance, the groups of Rezvani had prepared organic-inorganic hybrid nanocatalysts based Anderson-type polyoxometalate *via* a sol-gel method. 94% desulfurization efficiency was reached in 2 h with $((C_4H_9)_4N)_6Mo_7O_{24}$/PVA as catalyst at 313 K [11]. Additionally, vanadium-substituted Dawson-type polyoxometalate $[cetronium]_{11}P_2W_{13}V_5O_{62}$ had been prepared and employed in the oxidative desulfurization. 90% sulfur was removed from 500 ppm fuels with H_2O_2 as oxidant [12]. It is worth noting that Keggin-type POMs-based catalysts are significant interest on desulfurization [13]. Recently, 97% desulfurization efficiency was reached using organic-inorganic hybrid compound PWMn/NiO/PAN catalysts within 1 h at 308 K [14]. Nevertheless, less investigations on removing sulfur compounds using Lindqvist-type POMs ($[Mo_6O_{19}]^{n-}$ (n=2)) as catalysts was reported [15]. Furthermore, TiO_2 has been extensively used as a good carrier to prepare the heterogeneous catalysts due to high specific area, high yield and strong adsorptive ability for sulfur atoms with lone pair electrons [16, 17]. A series of phosphotungstic acid/TiO_2 (HPW/TiO_2) nanocomposites had been synthesized and applied in oxidative desulfurization. 95.2% conversion efficiency of sulfur-containing compounds was reached with HPW/TiO_2 (20 wt%) as catalysts at 333 K within 2 h [18]. Sulfur-containing compounds could be removed completely with 0.03 g phosphotungstic acid/TiO_2 as catalyst at 323 K [19]. Combining with the beneficial properties of TiO_2 carrier and Lindqvist-type POMs active species, it is expected that Lindqvist-type POMs-based TiO_2 catalysts would present high desulfurization performance.

In this work, the amphipathic Lindqvist-type polyoxometalate-based TiO_2 nanofibres containing quaternary ammonium cations was synthesized by combination with electrospinning and impregnation method. Different characterizations were taken to investigate the structure, compose and morphology of the catalysts. The impact of the critical parameters (catalysts types, temperatures, O/S molar ratios and substrates) was systematically evaluated using Box-Behnken experimental design. Additionally, the recycling property of catalysts was investigated, and the possible mechanism of ECODS was also studied.

2 Material and Methods

2.1 Chemicals

1-butyl-3-methylimidazolium hexafluorophosphate ([Bmim]PF_6) was synthesized according to literature [20]. Tetrabutyl ammonium bromide (TBA·Br), dodecyl trimethyl ammonium bromide (DTA·Br), hexadecyl trimethyl ammonium bromide (HTA·Br) and octadecyl trimethyl ammonium chloride (OTA·Cl) were purchased from Energy Chemical. Benzothiophene (BT), dibenzothiophene (DBT) and 4,6-dimethyl-dibenzothiophene (4,6-DMDBT) were received from China Pingmei Shenma Energy & Chemical Group Co., Ltd. Dichloromethane, n-octane, N,N-dimethylformamide (DMF) and Tetrabutyl titanate ($Ti(OC_4H_9)_4$) were procured from Tianjin GuangFu Fine Chemical Research Institute. And biphenyl was received from Sinopharm Chemical Reagent Co., Ltd. Polyvinyl pyrrolidone (PVP, M_W = 1300000) was purchased from Aladdin. Hydrogen peroxide (H_2O_2, 30 wt.%), acetylacetone and acetic acid were obtained from Beijing Chemical Works. All the chemicals were directly used as received without further purification.

2.2 Preparation of Catalysts

The detailed synthetic processes of DTA-MoO and TiO_2 nanofibres were depicted in Supplementary Information. A typical synthesis of **50-DTA-MoO-TiO_2 NF** was carried out as following: 0.10 g of TiO_2 nanofibres were dispersed in 50.00 mL anhydrous ethanol with magnetic stirring for 30 min, which was marked as solution A. Solution B was the mixture of 0.10 g DTA-MoO and 50.00 mL anhydrous ethanol. Subsequently, solution B was slowly added to solution A under stirring (700 rpm), and the precipitates were obtained. Finally, the abovementioned precipitate was washed with ethanol three times and dried at 80 °C in vacuum oven overnight. All catalysts were prepared with this similar processes: **50-TBA-MoO-TiO_2 NF**: 50 wt.% TBA-MoO-TiO_2 nanofibres; **50-OTA-MoO-TiO_2 NF**: 50 wt.% OTA-MoO-TiO_2 nanofibres; **50-HTA-MoO-TiO_2 NF**: 50 wt.% HTA-MoO-TiO_2 nanofibres; **30-DTA-MoO-TiO_2 NF**: 30 wt.% DTA-MoO-TiO_2 nanofibres; **40-DTA-MoO-TiO_2 NF**: 40 wt.% DTA-MoO-TiO_2 nanofibres; **60-DTA-MoO-TiO_2 NF**: 60 wt.% DTA-MoO-TiO_2 nanofibres.

2.3 Desulfurization Process

Model oil with 500 ppm S was prepared by dissolving DBT (or BT or 4,6-DMDBT) in n-octane. Biphenyl was internal standard. In a typical running, the water bath was firstly heated to the desired temperature. 5 mL of model oil and 1 mL of IL ([Bmim]PF_6) were mixed in round-bottom flask, and stirred 15 min at the desired temperature water bath. A certain amount of catalysts was added into the above flask. Subsequently, 11 μL of 30 wt.% H_2O_2 was added into the mixture under stirring and started the reaction. After the reaction, the model oil was analyzed by GC-FID (Agilent 7820A; DB-5, 30 m × 0.32 mm i.d. × 0.25 μm; FID: Agilent). The other desulfurization experiments were executed by the same process besides different temperatures, O/S molar ratios and dosages of catalysts.

2.4 Characterization of the Catalysts

The actual loading amounts of DTA-MoO on TiO_2 nanofibres were examined by the Leeman Prodigy Spec inductively coupled plasma atomic emission spectrometer (ICP-AES). The morphology of catalysts was analyzed by Hitachi SU8010 field emission scanning electron microscope (FE-SEM). The JEM-2010 transmission electron microscope with 200 kV working voltage was employed to finish transmission electron microscope (TEM) analysis, and the images were acquired by Gatan multiople CCD camera in detail. XRD analysis was carried out using Rigaku D/max-RA XRD diffractometer in the range of 2θ from 5° to 80°. The Fourier transform infrared spectra (FT-IR) of catalysts was collected by a Mattson Alpha-Centauri Fourier transform infrared spectrometer using KBr Pelles, the range was fixed in 4000–400 cm^{-1}, the number of scan was 64 and the resolution was 4 cm^{-1}. Thermogravimetric (TG) measurement was expressed on a Perkin-Elmer TGA 7 instrument with a heating rate of 10 °C·min^{-1} in air. The elemental mapping of catalysts was recorded by OXFORD ISIS-300 energy dispersive spectrometer.

3 Results and Discussion

3.1 Catalysts Characterization

Fig. 1 clearly demonstrated that both the diffraction peaks of anatase TiO_2 (lattice plane (101) located in about 25 °, PDF#71-1166) and rutile TiO_2 (lattice plane (110) located in about 27 °, PDF#75-1749) were appeared in XRD patterns of **30-DTA-MoO-TiO_2 NF**, **40-DTA-MoO-TiO_2 NF**, **50-DTA-MoO-TiO_2 NF** and **60-DTA-MoO-TiO_2 NF** in the scope of 2θ from 5 ° to 80 °. These results indicated that these catalysts were the mixed-phase of rutile and anatase TiO_2 [21]. The diffraction peaks in the range of 5–15° (the dotted box in Fig. 1) for **x wt%-DTA-MoO-TiO_2 NF** (x = 30, 40, 50 and 60) catalysts were observed and assigned to DTA-MoO, which indicated that DTA-MoO was present in the catalysts [22]. However, the position of MoO-POMs characteristic peaks for **x wt%-DTA-MoO-TiO_2 NF** (x = 30, 40, 50 and 60) shifted compared that of pure MoO-POMs, as shown in Fig. 1. This result indicated that the interaction between DTA-MoO and TiO_2 nanofirbres was existed for **x wt%-DTA-MoO-TiO_2 NF** (x = 30, 40, 50 and 60) catalysts. Additionally, the XRD patterns of bare TiO_2 nanofibres, **50-TBA-MoO-TiO_2 NF**, **50-OTA-MoO-TiO_2 NF** and **50-HTA-MoO-TiO_2 NF** was proved in Fig. S1. The

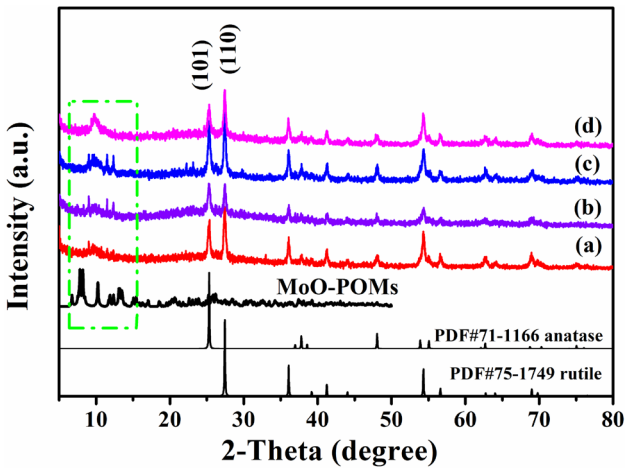

Fig. 1 XRD patterns of (**a**) **30-DTA-MoO-TiO_2 NF**, (**b**) **40-DTA-MoO-TiO_2 NF**, (**c**) **50-DTA-MoO-TiO_2 NF** and (**d**) **60-DTA-MoO-TiO_2 NF** with the standard cards of anatase and rutile phase TiO_2 and MoO-POMs

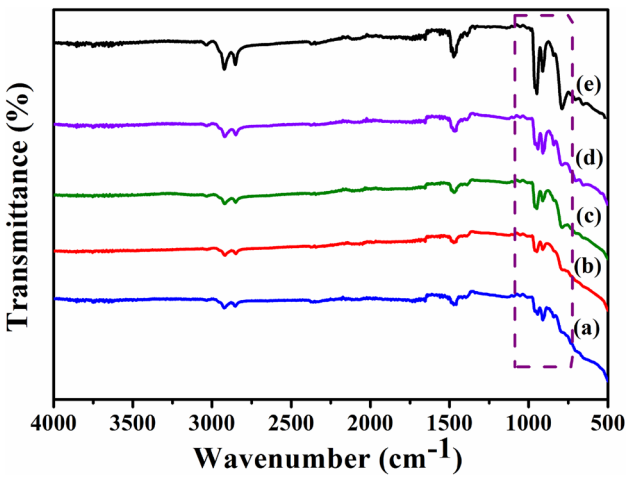

Fig. 2 FT-IR spectra of (**a**) **30-DTA-MoO-TiO_2 NF**, (**b**) **40-DTA-MoO-TiO_2 NF**, (**c**) **50-DTA-MoO-TiO_2 NF**, (**d**) **60-DTA-MoO-TiO_2 NF** and DTA-MoO (**e**)

crystalline phase of TiO_2 was still mixed-phase structure of anatase and rutile for bare TiO_2 nanofibres, **50-TBA-MoO-TiO_2 NF**, **50-OTA-MoO-TiO_2 NF** and **50-HTA-MoO-TiO_2 NF**, respectively. The results indicated that the loading of DTA-MoO, TBA-MoO, OTA-MoO and HTA-MoO cannot influence the original crystalline phase of TiO_2.

As could be seen in Fig. 2, the characteristic peaks (in the purple dotted box) located in 956, 834, 779 and 646 cm^{-1} were ascribed to the characteristic modes of ν (Mo = O(t)), ν (Mo-O(b)-Mo) and ν(Mo-O(c)-Mo), respectively [23]. All abovementioned bands were observed from 1000 to 600 cm^{-1} of the FT-IR spectra of **x wt% DTA-MoO-TiO_2 NF** (x = 30, 40, 50 and 60), suggesting that the Lindqvist-type POMs structure was preserved in the catalysts. However, the position of POMs characteristic peaks for **x wt% DTA-MoO-TiO_2 NF** (x = 30, 40, 50 and 60) shifted compared that of pure POMs, as seen in Fig. 2. The regions from 500 to 2000 cm^{-1} in FT-IR spectra were expanded to clearly show the characteristic peaks of POMs for all materials, which was shown in Fig. S2. The bending vibration appeared at 1430 cm^{-1} corresponding to the presence of Ti-O bond of TiO_2 [24]. It was clear that the peaks became more intense and the slightly shifted with the increasing of DTA-MoO content in these as-prepared samples. This phenomenon attributed to the strong interaction between DTA-MoO and TiO_2 [18]. It was accepted that the presence of water could be confirmed by the absorption band at 1632 cm^{-1}, which was associated with H-O-H bending movement from surface-absorbed water [25]. The bands at 1479, 2850 and 2915 cm^{-1} were rooted in the vibrations of quaternary ammonium cations [26]. Furthermore, Mo, C, O, Ti and N elements were detected in the EDS spectrum of **50-DTA-MoO-TiO_2 NF** (Fig. S3), which was in accordance with the results of FT-IR analysis. The loading amounts of DTA-MoO on TiO_2 nanofibres were measured by ICP elemental analysis, which was closed to the expected values (Table S1). The real values of DTA-MoO loading were 27 wt.%, 30 wt.%, 40 wt.% and 51 wt.% for **30-DTA-MoO-TiO_2 NF**, **40-DTA-MoO-TiO_2 NF**, **50-DTA-MoO-TiO_2 NF** and **60-DTA-MoO-TiO_2 NF**, respectively. Also, the real loading values for **50-TBA-MoO-TiO_2 NF**, **50-OTA-MoO-TiO_2 NF** and **50-HTA-MoO-TiO_2 NF** were also characterized and listed in table S1. These results suggested that the different cations-MoO was loaded on the TiO_2 nanofibres successfully, and Lindqvist-type MoO POMs structure was remained.

The states of Mo and Ti in **50-DTA-MoO-TiO_2 NF** were further characterized at the molecular level by XPS spectra. As shown in Fig. 3A, the peaks at 232.75 and 235.91 eV were assigned to Mo $3d_{5/2}$ and Mo $3d_{3/2}$, respectively. Mo(VI) was presented in **50-DTA-MoO-TiO_2 NF** [27]. Two peaks of 458.85 and 464.47 eV (Fig. 3B) were attributed to Ti $2p_{3/2}$ and Ti $2p_{1/2}$, respectively, which was consistent with the reported data of TiO_2. Ti(IV) was in presented in **50-DTA-MoO-TiO_2 NF** [28].

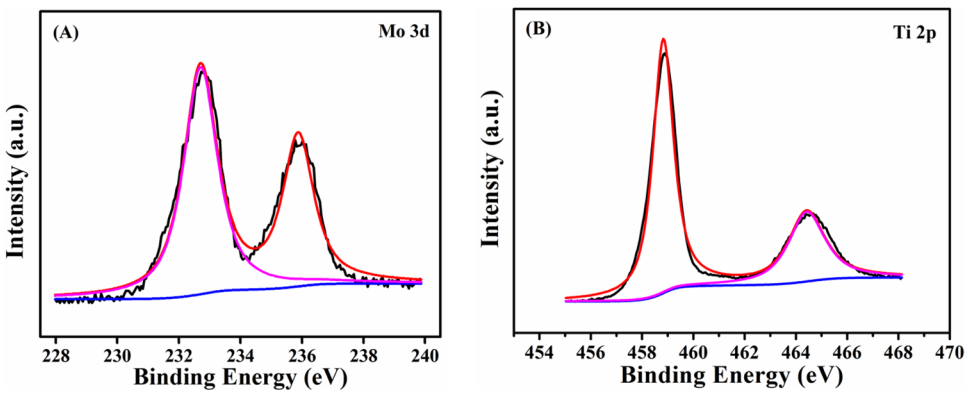

Fig. 3 XPS spectra of **50-DTA-MoO-TiO_2 NF**, (**a**) Mo 3d and (**b**) Ti 2p

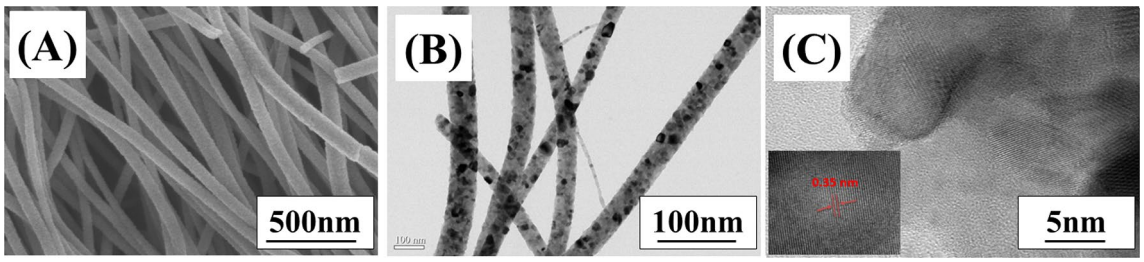

Fig. 4 (**a**) FE-SEM image of **50-DTA-MoO-TiO_2 NF**, (**b**) TEM image of **50-DTA-MoO-TiO_2 NF**, (**c**) HR-TEM image of **50-DTA-MoO-TiO_2 NF** (inset is the lattice fringe of lattice spacing of (101) plane in the anatase phase TiO_2)

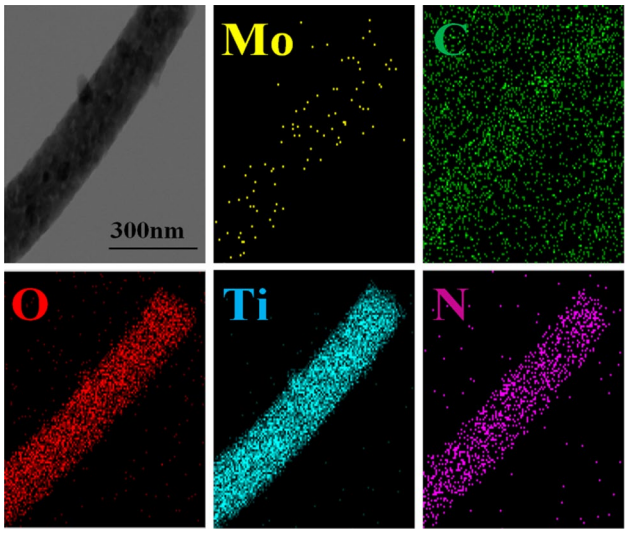

Fig. 5 TEM image of representative signal nanofiber of **50-DTA-MoO-TiO_2 NF** and corresponding elemental mapping of Mo (yellow), C (green), O (red), Ti (cyan) and N(pink)

Table 1 Effect of various desulfurization systems and catalysts on desulfurization efficiency.

Entry	Catalyst	Oxidant	Extractant	Desulfurization efficiency (%)
1	No	H_2O_2	No	3
2	No	No	[Bmim]PF_6	7
3	**50-DTA-MoO-TiO_2 NF**	H_2O_2	No	84
4	**50-DTA-MoO-TiO_2 NF**	No	[Bmim]PF_6	33
5	**50-DTA-MoO-TiO_2 NF**	H_2O_2	[Bmim]PF_6	100
6	MoO	H_2O_2	[Bmim]PF_6	45
7	[a]TiO_2 nanofibres	H_2O_2	[Bmim]PF_6	21
8	[b]DTA-MoO	H_2O_2	[Bmim]PF_6	85
9	[c]DTA-MoO+TiO_2 NF	H_2O_2	[Bmim]PF_6	67

Reaction conditions: DBT as desulfurization substrate, T = 333 K, m_{cat} = 0.010 g, O/S = 2:1, t = 40 min. [a]TiO_2 nanofibres and [b]DTA-MoO: the preparation processes were presented in Supplementary Information. [c]DTA-MoO+TiO_2 NF was the physical mixing of DTA-MoO and TiO_2 nanofibres.

As shown in Fig. 4A, the fiber-like was uniformly dispersed in the ambient environment. The diameter of **50-DTA-MoO-TiO_2 NF** was about 70 nm. More structural information of **50-DTA-MoO-TiO_2 NF** can be obtained by TEM analysis (Fig. 4B). The results indicated that the morphology of **50-DTA-MoO-TiO_2 NF** was fiber-like and the diameter was the same to the result of SEM. The large areas

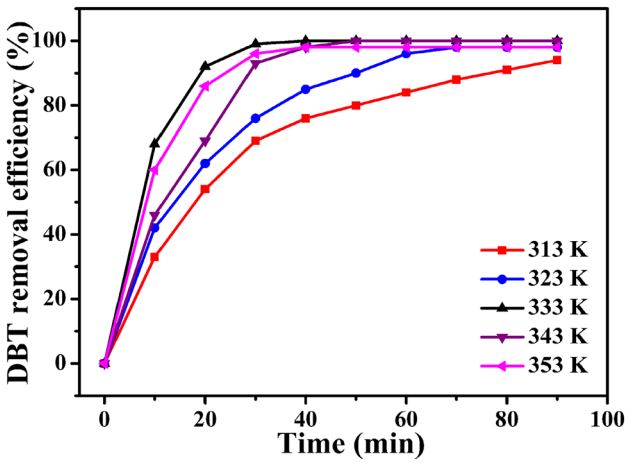

Fig. 6 Influence of reaction temperature on DBT removal efficiency, reaction conditions: O/S = 2:1, m_{cat} = 0.010 g

of samples were occupied by so many black spots remarkably, which were the POMs active sites. This indicated that DTA-MoO was dispersed uniformly. The detailed information was further confirmed *via* HR-TEM. In Fig. 4C, the lattice fringes for phase determination is 0.35 nm (in Fig. 4C inset), corresponding to the lattice spacing of (101) plane in the anatase phase TiO_2, which was clearly observed. Furthermore, the excellent dispersion of active species was evidenced by the elemental mapping of **50-DTA-MoO-TiO_2 NF** (Fig. 5). The elements of Mo, C, O, Ti and N were detected, and this result was in accordance with that for EDS. Furthermore, Mo was evenly scattered in the TiO_2 nanofibers. Moreover, the thermal stability of **50-DTA-MoO-TiO_2 NF** was investigated by TG, and the result was shown in Fig. S4. It indicated that **50-DTA-MoO-TiO_2 NF** was excellent stability.

3.2 Effect of Various Desulfurization Systems and Catalysts on DBT Removal Efficiency

DBT was a representative aromatic sulphur-containing compound, which was also one of the main refractory sulphur-containing compounds in HDS treatment. Therefore, DBT was selected as a main desulfurization substrate to study the effect of various desulfurization systems and catalysts types on desulfurization efficiency. As could be seen from Entry 1-4 in Table 1, the desulfurization efficiencies were 3%, 7%, 84% and 33% for ODS (Entry 1), EDS (Entry 2), oxidative catalytic desulfurization system (OCDS, Entry 3) and extractive catalytic desulfurization system (ECDS, Entry 4), respectively. Nevertheless, when **50-DTA-MoO-TiO_2 NF**, [Bmim]PF_6 and H_2O_2 were together applied in desulfurization reaction, 100% desulfurization efficiency was realized under the same conditions (Entry 5, Table 1).

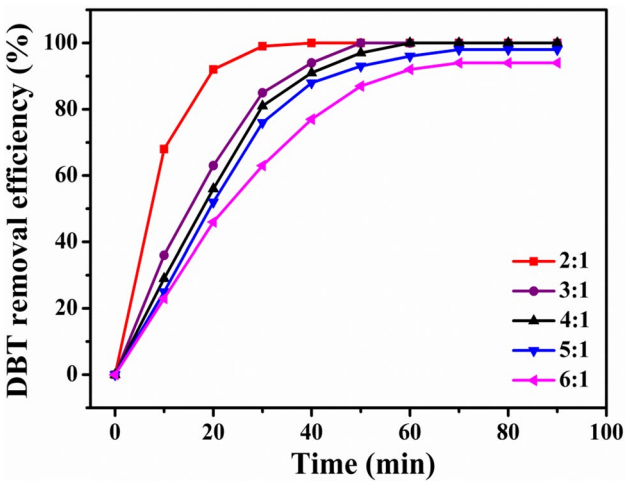

Fig. 7 Effect of O/S molar ratio on removal efficiency of DBT, reaction conditions: T = 333 K, m_{cat} = 0.010 g

Table 2 The sulfur removal in desulfurization process with various n(O/S).

Entry	Catalyst	n (O/S)	Sulfur removal/%	Ref.
1	HPW/TiO_2	12	100	[33]
2	PW_{12}/TiO_2	12	95.2	[18]
3	$FeCl_3$	6	96.1	[34]
4	Ti-MSM	10	99.8	[35]
5	PW_{12}/mpg-C_3N_4	8	100	[36]
6	$[(C_8H_{17})_3NCH_3]Cl/FeCl_3$	14	97.9	[37]
7	$Na_2MoO_4{\cdot}2H_2O$	4	99	[38]
8	**50-DTA-MoO-TiO_2 NF**	2	100	This work

The desulfurization efficiencies of MoO (Entry 6), TiO_2 nanofibres (Entry 7), DTA-MoO (Entry 8) and DTA-MoO+TiO_2 NF(Entry 9) as catalyst were 45%, 21%, 85% and 67%, respectively. These experimental results showed that the supported polyoxometalate-based catalyst was more active than the unsupported polyoxometalate catalyst. The excellent catalytic ability of **50-DTA-MoO-TiO_2 NF** was also verified comparing to previous reported ones (Table S2). The results implied that the interaction between DTA-MoO and TiO_2 nanofibres made for higher catalytic activity. At the same time, TiO_2 nanofibres as supporter can promote the dispersion of catalytic sites. Therefore, ECODS and **50-DTA-MoO-TiO_2 NF** was selected as the appropriate desulfurization system and catalyst, respectively.

3.3 Influence of Reaction Temperature and Time on DBT Removal Efficiency

Reaction temperature played a vital role in desulfurization efficiencies [29]. The influence of temperature on desulfurization performance was investigated and the results were depicted in Fig. 6. The removal efficiency of DBT increased from 94% at 313 K to 98% at 323 K within 90 min. It could be found that the sulfur-containing compounds were almost eliminated when the temperature was raised, which was associated with increasing of active species with the increasing temperature [30]. Besides, ILs viscosity decreases with the temperature increasing from 313K to 333K, and then favours the extraction of DBT from oil to cause an improvement of desulfurization efficiency. Nevertheless, the time to completely eliminate DBT could be lengthened from 40 to 50 min when the temperature was 333 and 343 K. However, 98% desulfurization efficiency was obtained at 353 K in the same condition. Increasing the temperature from 333 to 353 K did not have a significant effect on the rate of reactions. This phenomena could be explained that the relative higher temperature would cause thermal self-decomposition of H_2O_2 [31]. Additionally, the highest desulfurization efficiency was recorded after 90 min. Therefore, the temperature and reaction time were conducted at 333 K and 90 min under the current reaction conditions, respectively.

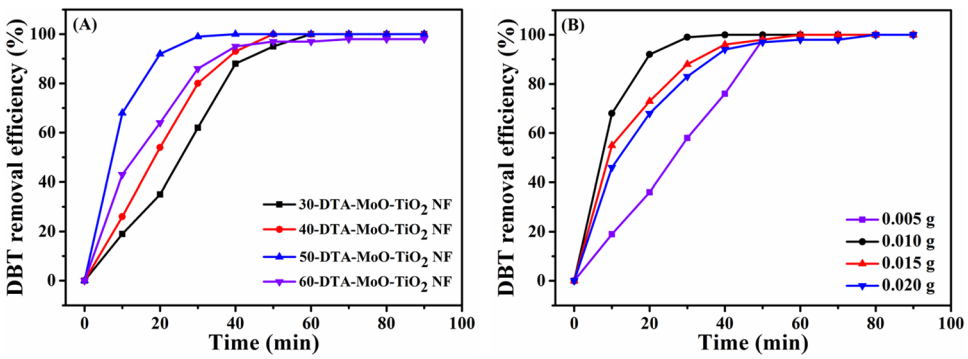

Fig. 8 (**a**) Effect of loading amount of DTA-MoO on DBT removal efficiency, reaction conditions: O/S = 2:1, m_{cat} = 0.010 g, T = 333 K; (**b**) Effect of catalyst dosage on DBT removal efficiency, reaction conditions: O/S = 2:1, T = 333 K

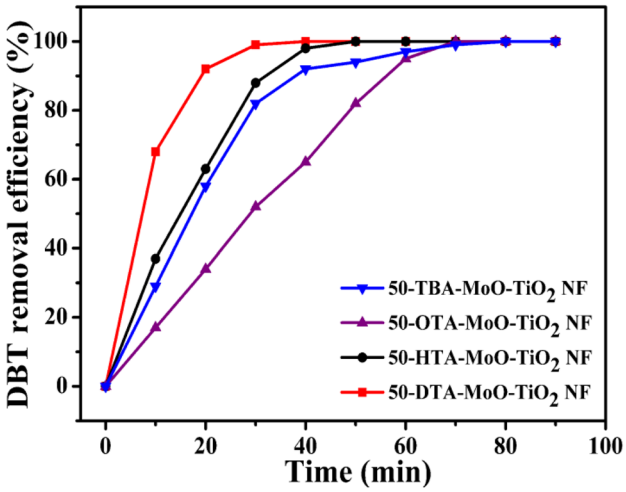

Fig. 9 Influence of different counter cations in catalyst on DBT removal efficiency, reaction conditions: T = 333 K, m_{cat} = 0.010 g, O/S = 2:1

3.4 Effect of O/S Molar Ratio on DBT Transformation Efficiency

Effect of O/S molar ratio on desulfurization efficiency was investigated in the range of 2:1 to 6:1 (Fig. 7). As can be seen from Fig. 7, 40 min was consumed to achieve the complete removal of sulfur-containing compounds under 2:1 of O/S molar ratio. When the O/S molar ratio was 3:1, 4:1, 5:1 and 6:1, the desulfurization efficiency of 100%, 100%, 98%, and 94% was realized in 50, 60, 90 to 90 min, respectively. With H_2O_2 usage increasing, desulfurization efficiencies showed a downward trend, and the consumption time was longer. It was due to forming a liquid film by adding more H_2O_2 and make it hard to approach sulfur-containing compounds. According to the stoichiometric reaction, 2 mol H_2O_2 is consumed for oxidizing 1 mol sulphur-containing compound to corresponding sulfone [32]. To our delight, the O/S molar ratio in this work was coincident with stoichiometry. The experimental safety was guaranteed in the mild reaction conditions with small dosage of H_2O_2. It was meaningful at this point to compare the value of O/S molar ratio by previous literatures (Table 2). This result confirmed that amphipathic catalysts played a significant role in improving H_2O_2 utilization rate. In detail, TiO_2 nanofibres with prominent hydrophilic feature connected with tiny amount of H_2O_2 conveniently, and the hydrophobic characteristic of carbon chain provided the excellent accessibility for sulfur atom. Consequently, 2:1 was the most proper O/S molar ratio with regard to the safety, economic consideration and desulfurization performance.

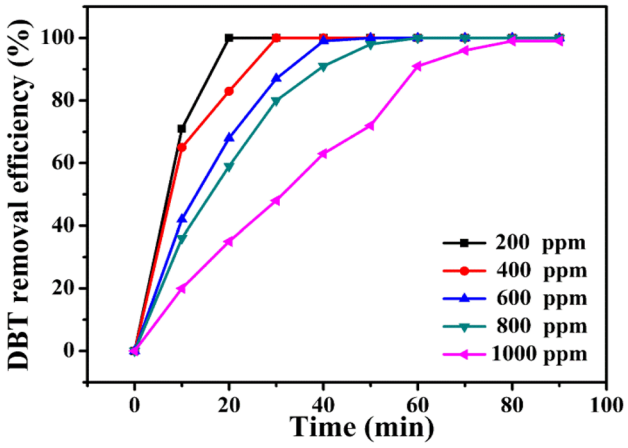

Fig. 10 Influence of initial concentration of DBT on desulfurization efficiency, reaction conditions: T = 333 K, m_{cat} = 0.010 g, O/S = 2:1

3.5 Effect of Loading Amount of DTA-MoO and Catalyst Dosage on DBT Removal Efficiency

Many reports illustrated that the desulfurization efficiency was influenced by the availability and distribution of active species, which were crucially depended on the loading amounts of DTA-MoO and catalyst dosages in this work [39]. Thus, the desulfurization performance of catalysts with various loading amounts of DTA-MoO and catalysts dosages was investigated. As shown in Fig. 8A, 60, 70, and 40 min was consumed to remove DBT completely using **30-DTA-MoO-TiO_2 NF**, **40-DTA-MoO-TiO_2 NF** and **50-DTA-MoO-TiO_2 NF** as catalyst, respectively. While only 98% desulfurization efficiency was achieved with **60-DTA-MoO-TiO_2 NF** within 90 min. These results indicated that

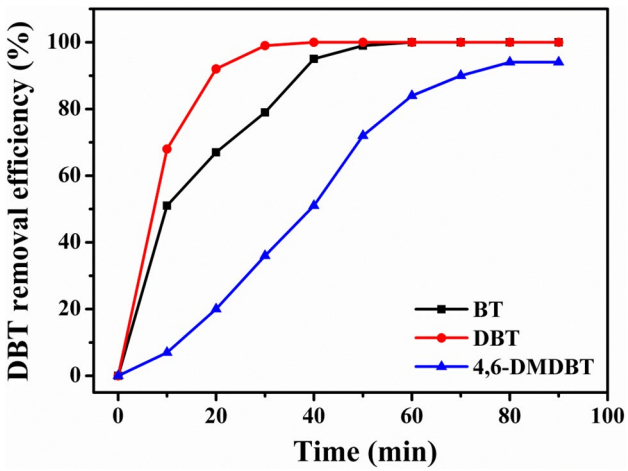

Fig. 11 Removal of various sulfur-containing compounds in desulfurization system, reaction conditions: T = 333 K, m_{cat} = 0.010 g, O/S = 2:1

50-DTA-MoO-TiO_2 NF presented the fastest desulfurization speed. The optimization dosage of the catalysts was researched by varying amount of **50-DTA-MoO-TiO_2 NF** from 0.005 to 0.020 g in ECODS. Fig. 8B displayed the different DBT removal efficiencies using different amounts of catalysts. The reaction time was drastically reduced with increasing catalyst dosage. It seemed that the increasing of catalysts amount was an efficient strategy to enhance desulfurization performance [40]. However, the reaction time was not reduced at high dosage(>0.010 g), which might be assigned to the agglomerate of catalysts to decrease available active sites [41]. The most favorable **50-DTA-MoO-TiO_2 NF** dosage was found to be 0.010 g for the forthcoming desulfurization process.

3.6 Influence of Different Counter Cations in Catalyst on DBT Removal Efficiency

As shown in Fig. 9, it consumed 80, 70, 50 and 40 min to achieve 100% desulfurization efficiency with **50-TBA-MoO-TiO_2 NF**, **50-OTA-MoO-TiO_2 NF**, **50-HTA-MoO-TiO_2 NF** and **50-DTA-MoO-TiO_2 NF** as catalysts, respectively. The result was probably attributed that the longer carbon chain formed an obstacle between sulfur compounds and active sites to hinder desulfurization reaction. On the contrary, with shorter carbon chain, DBT can easily get in touch with active sites due to relative smaller steric hindrance [42]. The activity order with various counter-ions decrease as following: $DTA^+ > HTA^+ > OTA^+ > TBA^+$. The result further verified **50-DTA-MoO-TiO_2 NF** was the most suitable catalyst for satisfying requirement of deep desulfurization.

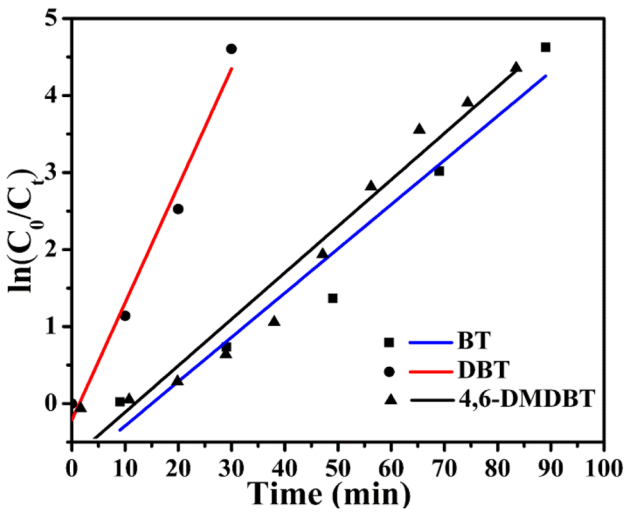

Fig. 12 The pseudo-first-order kinetics for oxidation of different substrates, reaction conditions: T = 333 K, m_{cat} = 0.010 g, O/S = 2:1

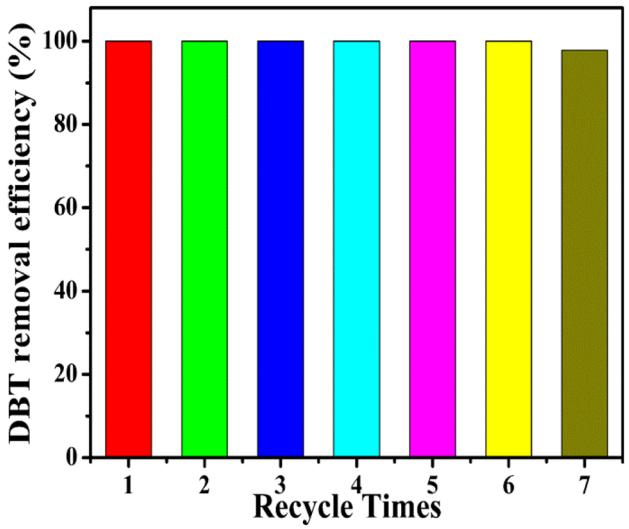

Fig. 13 Recycle performance of **50-DTA-MoO-TiO_2 NF** for removing DBT, reaction conditions: T = 333 K, m_{cat} = 0.010 g, O/S = 2:1

3.7 Influence of Initial Concentration of DBT on Desulfurization Efficiency

As shown in Fig. 10, with increasing of DBT concentration, the reaction time was prolonged for 100% desulfurization efficiency. This because that there were more DBT in oil needed to be converted. On the other hand, the amount of active sites was not enough to completely oxidize DBT into sulfones with the equal amount of **50-DTA-MoO-TiO_2 NF** and H_2O_2 [43]. Therefore, the desulfurization reaction rate increased with decreasing DBT concentration.

3.8 Removal of Various Sulfur-Containing Compounds in Desulfurization System

BT and 4,6-DMDBT as DBT derivants were also the typical inflexible sulfur-containing compounds. The removal efficiencies of above two sulfur-containing compounds were carried out and the results were showed in Fig. 11. 100% desulfurization efficiency could be achieved within 60 and 40 min for BT (S electron density 5.739) and DBT (S electron density 5.758), respectively. The lowest electron density of sulfur atom for BT displayed lowest reactivity. 4,6-DMDBT (S electron density 5.760) possessed the highest electron density among three sulfur-containing compounds, but only 94% desulfurization efficiency was obtained in 90 min under the same experimental conditions. 4,6-DMDBT was hindered to react with active species due to the steric hindrance of methyl groups in 4,6-DMDBT, and then the desulfurization efficiency reduced. As such, the removal efficiencies for various substrates decreased in the order of DBT > BT > 4,6-DMDBT. Such an order in the removal

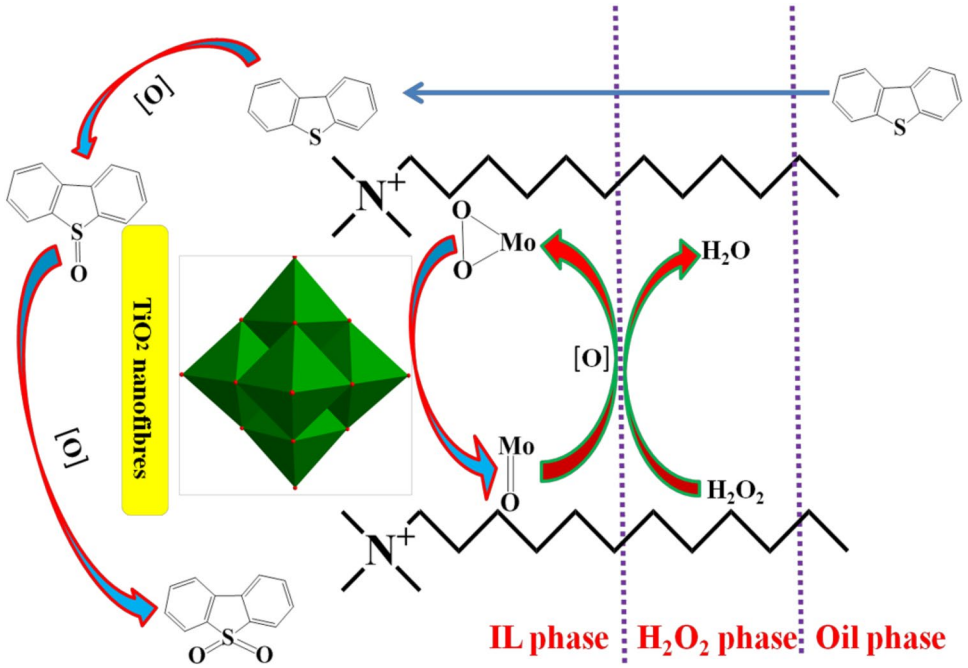

Fig. 14 Proposed desulfurization mechanism of **50-DTA-MoO-TiO_2 NF** in ECODS with three-liquid-phase system

efficiency of different substrates was agreed well with that reported in ECODS system [14]. We concluded that the desulfurization efficiencies of various substrates was correlated to the electronic density of the S-atom and the steric hindrance [32].

The oxidation kinetics of DBT, 4,6-DMDBT and BT were also investigated under the optimal conditions with **50-DTA-MoO-TiO_2 NF** as catalyst. The rate constants, half-lives and correlation coefficient were obtained from the pseudo-first-order equation [44].

$$-\mathrm{d}c/\mathrm{d}t = kc \tag{1}$$

$$\ln\left(c_0/c_t\right) = kt \tag{2}$$

$$t_{1/2} = 0.693/k \tag{3}$$

It is noted that c_0 and c_t were the sulfur concentrations at 0 min and t min, respectively, and k was the first-order rate constant (min^{-1}). In Fig. 12, the plot of $\ln(c_0/c_t)$ versus time was the linear. The half-lives were calculated *via* Eq.(3). These results indicated that desulfurization reaction with **50-DTA-MoO-TiO_2 NF** as catalysts was a pseudo-first-order reaction.

3.9 Recycling

The recyclability of catalysts was fatal for industrial applications. Therefore, the recycling performance of **50-DTA-MoO-TiO_2 NF** was investigated under optimum conditions. After reaction, the upper oil was poured out carefully. And then dichloromethane was used to extract $DBTO_2$ from ILs because of the limited extraction ability of ILs. ILs and catalysts (dispersed into ILs) were stayed in round-bottom flask for the next reaction after evaporating and drying in vacuum at 80 °C for 24 h. The fresh model oil and H_2O_2 were added and the new desulfurization reaction began. The slight decrease of DBT removal efficiency was observed after seven recycle (Fig. 13). For one thing, the oxidative product DBT ($DBTO_2$) continuously enriched and covered on the surface of the catalysts, which deactivated the active sites [45]. For another, slow leaching of the active species was inevitable in separation process [46]. The catalysts were appropriate and feasible for practical industrial application, thereby suggesting the promising value of ECODS in this work.

3.10 Mechanism

In Fig. 14, the model oil located in the upper layer (containing DBT), H_2O_2 was contained in the middle layer, and **50-DTA-MoO-TiO_2 NF** was dispersed in the ILs ([Bmim]PF_6, in the lowest layer). The ECODS was consisted of three phases because that [Bmim]PF_6 ILs was not dissolved in the water [47]. After stirring, these three phases was thoroughly mixed together. DBT was firstly extracted from the oil phase into ILs phase. At the same time, the active species [abbreviated as $Mo(O_2)$] were obtained by MoO in **50-DTA-MoO-TiO_2 NF** reacting with H_2O_2. Subsequently, DBTO was gained by oxidizing DBT with one

[O] deriving from $Mo(O_2)$. DBTO was further reacted with $Mo(O_2)$ to form $DBTO_2$, and then $Mo(O_2)$ returned back to Mo=O continuously until H_2O_2 was exhausted totally [6, 48]. Finally, the higher polar $DBTO_2$ was still retained in the ILs phase and the clean fuels were obtained. ILs acted as extractant and reaction media, which also played a part in stabilizing active sites in desulfurization process [42].

4 Conclusions

The amphipathic Lindqvist-type polyoxometalate-based TiO_2 nanofibres were successfully prepared and as heterogeneous catalysts applied in removal of three sulfur compounds (BT, DBT and 4,6-DMDBT). As a result, at 333 K, 100% desulfurization efficiency for 500 ppm DBT model oil was achieved using 0.010 g **50-DTA-MoO-TiO_2 NF** as catalysts in 40 min. It is worth mentioning that the dosage of H_2O_2 (O/S molar ratio = 2:1) was exceptionally low. Prominent catalytic activity and high utilization rate of H_2O_2 were associated with amphipathic catalysts. In addition, desulfurization efficiencies of various substrates decreased in the following order: DBT > BT > 4,6-DMDBT. The desulfurization efficiency had the slight decrease until recycling 7 times.

Acknowledgements We acknowledged for the financial support from the NSF of China (21271038, 21571032), the China High-Tech Development 863 Program (2007AA03Z218), Youth Project of the Universities in Liaoning Province (LQN201719) and Doctoral Research Start-up Fund Project of Liaoning Provence (2019-BS-215). Furthermore, the excellent platform of analysis was provided by the Northeast Normal University, we expressed appreciate for these help. There are no conflicts of interest for each contributing author.

References

1. Tian YS, Wang GH, Juan L et al (2016) Chin J Catal 37:2098–2105
2. Zhang M, Liu JQ, Li HP et al (2020) Appl Catal B-Environ 271:118936–118944
3. Zhao K, Cheng H, Liu C et al (2015) RSC Adv 5:66013–66023
4. Shi YW, Zhang XW, Liu GZ (2015) ACS Sustain Chem Eng 3:2237–2246
5. Dou SY, Wang R (2019) Chem Eng J 369:64–76
6. Hu YW, He QH, Zhang Z et al (2011) Chem Commun 47:12194–12196
7. Ding WJ, Zhu WS, Xiong J et al (2015) Chem Eng J 266:213–221
8. Xu Y, Ma WW, Dolo A et al (2016) RSC Adv 6:66841–66846
9. Shen C, Wang YJ, Xu JH et al (2016) Green Chem 18:771–781
10. Ma WW, Xu Y, Ma KW et al (2016) Appl Catal A Gen 526:147–154
11. Rezvani MA, Asli MAN, Oveisi M et al (2016) RSC Adv 6:53069–53079
12. Banisharif F, Dehghani MR, Capel-Sanchez MC et al (2017) Ind Eng Chem Res 56:3839–3852
13. Cherevan AS, Nandan SP, Roger I et al (2020) Adv Sci 7:1903511–1903535
14. Rezvani MA, Miri OF (2019) Chem Eng J 369:775–783
15. Magueres PL, Hubig SM, Lindeman SV et al (2000) J Am Chem Soc 122:10073–10082
16. Xun SH, Zheng D, Yin S et al (2016) RSC Adv 6:42402–42412
17. Xun SH, Zhu WS, Zheng D et al (2015) RSC Adv 5:43528–43536
18. Yan XM, Mei P, Lei JH et al (2009) J Mol Catal A Chem 304:52–57
19. Yue D, Lei JH, Peng Y et al (2018) Fuel 226:148–155
20. Carda-Broch S, Berthod A, Armstrong DW (2003) Anal Bioanal Chem 375:191–199
21. Ma WW, Xu Y, Ma KW et al (2017) Mol Catal 433:28–36
22. Rezvani MA, Shaterian M, Akbarzadeh F et al (2018) Chem Eng J 333:537–544
23. Sharma S, Ghosh SK, Kumar M et al (2015) Polyhedron 100:290–295
24. Guo Y, Fu JW, Li L et al (2018) Inorg Chem Front 5:2205–2211
25. Wu L, Yu JC, Zhang L et al (2004) Sol State Chem 177:2584–2590
26. Lv HY, Deng CL, Ren WZ et al (2014) Fuel Process Technol 119:87–91
27. Kocijan A, Milosev I, Pihlar B (2004) J Mater Sci Mater Med 15:643–650
28. Palanisamy B, Badu CM, Sundaravel B et al (2013) J Hazard Mater 25:233–242
29. Bazayari A, Khodadadi AA, Mamaghani AH et al (2016) Appl Catal B 180:65–77
30. Zhang J, Wang AJ, Li X et al (2011) J Catal 279:269–275
31. Collins FM, Lucy AR, Sharp C (1997) J Mol Catal A Chem 117:397–403
32. Fu JW, Guo Y, Ma WW et al (2018) J Mater Sci 53:15418–15429
33. Zhu MY, Luo GQ, Kang LH et al (2014) RSC Adv 4:16769–16776
34. Zhang JT, Zhu WS, Li HM et al (2009) Green Chem 11:1801–1807
35. Shah AT, Li B, Abdalla ZE (2009) J Colloid Interface Sci 336:707–711
36. Hu XF, Lu YK, Dai FN et al (2013) Microporous Mesoporous Mater 170:36–44
37. Jiang YQ, Zhu WS, Li HM et al (2011) Chem Sus Chem 4:399–403
38. Zhu WS, Li HM, Jiang X et al (2008) Green Chem 10:641–646
39. Lv H, Ren W, Wang H et al (2013) Appl Catal A 453:376–382
40. Saha BW, Kumar SM, Sengupta SL (2019) Chem Eng Sci 199:332–341
41. Yang ZH, Gui B, Zhou CX et al (2009) Chin J Appl Chem 26:1315–1319
42. Li H, Jiang X, Zhu WS et al (2009) Ind Eng Chem Res 48:9034–9039
43. Maity U, Selvin R, Basu JK et al (2012) J Nanoeng Nanomanuf 2:241–247
44. Zhang M, Zhu WS, Xun SH et al (2013) Chem Eng J 220:328–336
45. Qiu L, Cheng Y, Yang C et al (2016) RSC Adv 6(2016):17036–17078
46. Yang C, Zhao K, Cheng Y et al (2016) Sep Purif Technol 163:153–161
47. Xu JH, Zhao S, Ji YC et al (2013) Chem Eur J 19:709–715
48. Dai BL, Wu PW, Zhu WS et al (2016) RSC Adv 6:140–147

Affiliations

Jiawei Fu[1] · Wenwen Ma[1,2] · Yu Guo[1] · Xiaonan Li[1] · Haiyu Wang[1] · Chen Fu[1] · Hong Zhang[1]

[1] Institute of Polyoxometalate Chemistry, Department of Chemistry, Northeast Normal University, Changchun, Jilin 130024, P. R. China

[2] College of Chemistry and Chemical Engineering, Energy and Environmental Catalysis Institute, Shenyang Normal University, Shenyang, Liaoning 110034, P. R. China